Available online at www.sciencedirect.com
SCIENCE DIRECT®
Polymer 44 (2003) 7495–7504
polymer
www.elsevier.com/locate/polymer

Effect of composition and comonomer type on the rheology, morphology and properties of ethylene-α-olefin copolymer/polypropylene blends

M. Kontopoulou*, W. Wang, T.G. Gopakumar, C. Cheung

Department of Chemical Engineering, Queen's University, Kingston, ON, Canada K7L 3N6

Received 24 October 2002; received in revised form 22 August 2003; accepted 25 August 2003

Abstract

The rheology, morphology, thermal and mechanical properties of blends containing low molecular weight polypropylene (PP) and metallocene-based ethylene-α-olefin copolymers (ECs) have been investigated. Evaluation of the thermo-rheological properties of the blends showed that they are immiscible, both in the solid and melt state, over the whole range of compositions. Rheological properties were correlated to blend morphology, by using the Palierne emulsion model. The resulting low values of interfacial tension confirmed excellent compatibility between the phases.

Addition of ECs in PP resulted in significant ductility improvement. The transition from plastic to elastomeric properties coincided with phase inversion. The butene-based EC was found to be the most beneficial in terms of impact properties.

Fine morphologies, with sub-micron sizes of the dispersed phase, were obtained upon post-extrusion shearing of the blends.

Keywords: Polypropylene; ethylene-α-olefin copolymers; blends

1. Introduction

The advancements in single-site type (metallocene) catalyst technology realized during the early nineties represent a significant milestone in polyolefin development. Polymerization using metallocene catalysts facilitates efficient control of the molecular structure. The incorporation of various degrees of long chain branching results in polyolefins with very low densities, elastomeric characteristics and unique rheological properties [1–3]. This family of polyolefins includes polyethylenes copolymerized with various types of comonomers (ethylene-α-olefin copolymers). The reported number of applications of these polymers is continuously increasing and significant research has been devoted in the area of their blends with conventional polyolefins [4–7]. Impact modification of polypropylene, using ethylene-α-olefin copolymers in the place of traditionally used ethylene–propylene–rubbers (EPRs) has attracted particular attention [8–14].

In spite of the plethora of research on such blends, most of the existing work has focused on relatively low viscosity ratio blends of polypropylene with octene based ethylene-α-olefin copolymers and there are few systematic comparisons between the performance of octene-based copolymers and their butene-based counterparts. In addition, there are conflicting claims in the literature regarding the miscibility of these blends. Although it seems that in the majority of cases they are thermodynamically immiscible, it has been reported that butene-rich and hexene-rich copolymers are miscible with isotactic PP in the amorphous region [15–17] and that partial miscibility in blends of PP with ethylene–octene copolymers may exist at low copolymer contents (below 10%) [11,14].

Due to their relatively low molecular weight compared to traditional EPRs, one of the potential applications of ethylene-α-olefin copolymers (ECs) is in impact modification of low molecular weight polypropylene. This paper presents a critical comparison of the thermo-rheological properties, morphology and mechanical properties of systems containing isotactic polypropylene of low molecular weight (high melt flow rate) and two types of ethylene-α-olefin copolymers; butene and octene-based. Inferences about the compatibility and thermodynamic miscibility of these blends are made.

* Corresponding author. Tel.: +1-613-533-3079; fax: +1-613-533-6637.
E-mail address: kontop@chee.queensu.ca (M. Kontopoulou).

0032-3861/$ - see front matter © 2003 Elsevier Ltd. All rights reserved.
doi:10.1016/j.polymer.2003.08.043

2. Experimental

2.1. Materials

One injection molding grade isotactic polypropylene homopolymer with MFR = 35 g/10 min and two ethylene-α-olefin copolymers produced by metallocene catalysts were used. All materials were supplied by ExxonMobil Chemical and are commercially available. Their properties, as reported by the supplier, are summarized in Table 1. Blend compositions ranging from 10 to 70% by weight were prepared as described below. Antioxidant of 0.3% (Irganox B225 from Ciba-Geigy) was added to the blends to prevent degradation.

2.2. Blend preparation

Blends were produced using a Haake Polylab R600 batch internal mixer and a twin-screw co-rotating intermeshing extruder, model ZSK-30 by Werner and Pfleiderer, with a standard compounding configuration. The batch mixer was operated at 210 °C, with a rotor blade speed of 60 rpm. The total mixing time was 7 min. The extruder was equipped with seven heating zones. Temperatures along the barrel ranged from 170 °C for zone 1 (hopper) to 225 °C for zone 7 (die). The screw speed was 200 rpm and the mass flow rate 2 kg/h. Extruded strands were immersed in a trough containing cold water. All thermal and rheological characterization was carried out using batch mixed samples and extruded samples were used to confirm reproducibility. Mechanical properties were evaluated using extruded blends.

2.3. Differential scanning calorimetry (DSC)

A Perkin–Elmer DSC-6 apparatus was used to determine thermal properties. The heat history of the samples was eliminated by heating them at a rate of 10 °C/min and holding them for 1 min at 200 °C. Subsequently, the samples were cooled to 0 °C at a rate of 10 °C/min and the crystallization temperature and heat of crystallization were recorded. Melting temperatures and heats of fusion were determined during a second heating sequence.

Percent crystallinity of the individual components was calculated by using the formula $X\% = H_f/H_{f,c} \times 100$, where X is the degree of crystallinity, H_f is the heat of fusion of each component and $H_{f,c}$ the heat of fusion of the completely crystalline polymer, which is equal to 163 kJ/kg for PP and 293 kJ/kg for polyethylene.

Successive self-nucleation and annealing (SSA) [18] was performed using a Seiko series DSC according to the following procedure: samples were heated from 20 to 180 °C at a rate of 10 °C/min under nitrogen atmosphere and held for 3 min before cooling to 20 °C at 10 °C/min to create a standard thermal history. Due to the large difference in melting points, SSA was performed separately for the EC and PP components. The self-seeding and annealing temperature of (T_s) must be high enough to melt all the crystalline regions, except for small crystal fragments and/or nuclei that can later self-seed the polymer during cooling. The first T_s was selected as 80 °C for EC and 175 °C for PP [19]. Samples were heated from 20 to 80 °C for EC and from 20 to 175 °C for PP at a rate of 10 °C/min and held isothermally for 5 min before cooling down to 20 °C at a rate of 10 °C/min. Subsequently, the samples were heated at 10 °C/min to a temperature 5 °C lower than the previous T_s and held for 5 min before cooling down to 20 °C at 10 °C/min. The procedure was repeated with T_s being lowered in 5 °C intervals with respect to the previous step. The fractionation range was 40–80 and 140–175 °C for the EC and PP components, respectively. After completion of the fractionation, melting endotherms and crystallization exotherms were recorded at 10 °C/min.

2.4. Rheology

A controlled stress rheometer, ViscoTech by Reologica, with parallel plate fixtures (20 mm in diameter) was used in the oscillatory mode at a gap of 1 mm to measure linear viscoelastic properties as a function of angular frequency (ω). Temperatures ranged from 170 to 230 °C. All measurements were carried out under nitrogen atmosphere to prevent degradation or absorption of moisture. Stress sweeps were performed to ensure that all measurements were within the linear viscoelasticity regime.

2.5. Effect of shearing on morphology

Shearing experiments to evaluate the effect of simple shear flow on morphology were conducted by operating the controlled stress rheometer in the creep mode at constant shear stresses of 25, 50 and 100 Pa and a temperature of 210 °C. The parallel plates were used with a gap of 1.5 mm. After maintaining the shear flow for periods of time ranging from 10 to 40 min, the samples were kept at 210 °C for an

Table 1
Ethylene-α-olefin copolymer properties

Resin	Comonomer type	M_n (g/mol)	M_w (g/mol)	Comonomer content (%)	MFI/MFR (g/10 min)	Density (kg/m^3)
EBC	Butene	58,000	114,000	19.4	0.8/1.3	880
EOC	Octene	46,000	98,600	25.5	1.1/2.5	882

additional 10 min, to allow time for the morphology to relax and stabilize, before cooling down rapidly by blowing air. When the parallel plate geometry is used, shear rate increases along the radius from the centre, therefore for consistent analysis all images were taken from surfaces located at two thirds of the disk radius, tangent to the direction of shear, following the procedures outlined by Martin et al. [20].

2.6. Scanning electron microscopy

Samples were fractured under liquid nitrogen, stained in RuO_4 vapour (supplied by Polysciences Inc.) for 3 h at room temperature and microtomed by a Leica RM2155 Rotationsmikrotom, according to the procedures described by Brown and Butler [21]. Surfaces were coated with gold and observed using a JEOL 840 Scanning Electron Microscope. Images were analyzed using the SigmaScan Pro Image Analysis software. At least 250 particles were used to calculate average diameters.

2.7. Dynamic mechanical analysis (DMA)

The temperature dependence of tensile moduli and loss tangent, tan δ, was determined using the solids testing setup in the Viscotech rheometer and operating in the tensile mode between -100 and 60 °C. The frequency was set to 1 Hz, and the heating rate was 5 °C/min. Glass transition temperatures were obtained from the peak of the loss tan δ curve.

2.8. Mechanical property testing

Tensile tests were carried out in an INSTRON universal testing machine, model 4200/5566, according to ASTM D638. Sheets approximately 2 mm thick were prepared by compression molding. A die (Type M-III) constructed in accordance to ASTM D638M was used to construct the dog-bone shaped specimens. The crosshead speed was 50 mm/min. Five runs were carried out per blend and averages were calculated.

An ITP200 impact tester (Adelaide Testing Machines Inc.) at the notched Izod mode was used to measure impact energy. A table-top injection molding machine was used for preparing impact test specimens with dimensions of $80 \times 10 \times 4\ mm^3$ conforming to ASTM D256. Average impact energy was obtained from five tests.

3. Results and discussion

3.1. Rheology

The viscoelastic properties of the pure components are shown in Fig. 1(a) and (b). Large differences in complex viscosity are evident between PP and ECs, due to the difference in molecular weight. The octene-based EOC displays more prominent shear thinning, due to the presence of long chain branching. Long chain branching also results in enhanced elasticity, as depicted in Fig. 1b.

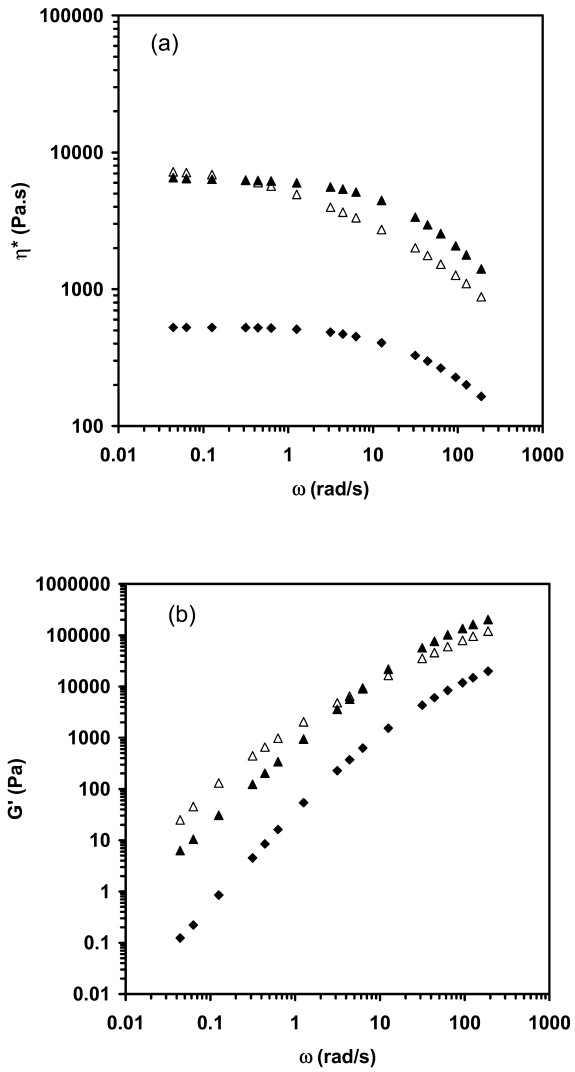

Fig. 1. Viscoelastic properties of pure components as a function of frequency (ω) at 210 °C (a) complex viscosity (η^*) (b) elastic modulus (G'); ▲ EBC, △ EOC, ◆ PP.

The Cross model [22], $\eta(\dot{\gamma}) = (\eta_0)/(1 + |\lambda\dot{\gamma}|^{n-1})$, was used to obtain fits of complex viscosity as a function of frequency for all blends: η is the viscosity corresponding to a shear rate $\dot{\gamma}$; η_0 the zero shear viscosity; λ a relaxation time related to the onset of non-Newtonian flow and associated to the longest relaxation time of the polymer melt; n is a measure of shear thinning. The Cross model parameters for all blend compositions are summarized in Table 2, together with the activation energies obtained by applying the Arrhenius expression [23]:

$$\eta_0 = A\, e^{\frac{\Delta E}{RT}} \tag{1}$$

where A is a constant characteristic of the polymer and its molecular weight, ΔE is the activation energy for viscous

Table 2
Cross model parameters at 210 °C and activation energies

Blend PP/EC	EBC				EOC			
	η_0 (Pa s)	λ (s)	n	E (kJ/mol)	η_0 (Pa s)	λ (s)	n	E (kJ/mol)
100/0	527	0.016	0.16	37.34	527	0.016	0.16	37.34
90/10	664	0.015	0.22	37.43	615	0.023	0.42	38.29
80/20	794	0.022	0.40	36.15	811	0.029	0.44	37.16
70/30	1104	0.030	0.48	36.07	1019	0.036	0.46	37.19
60/40	1213	0.021	0.36	35.10	1467	0.066	0.51	38.83
50/50	1808	0.023	0.34	37.51	2317	0.154	0.56	44.48
30/70	3692	0.026	0.28	34.71	6156	1.000	0.49	27.96
0/100	6478	0.028	0.24	29.79	8185	0.326	0.50	45.60

flow, R is the gas constant and T is the temperature in degrees Kelvin.

Generally, the pure components and their blends exhibit Newtonian plateaus over a wide range of frequencies, as evidenced by the short relaxation times obtained from the Cross model. The relaxation times for blends containing EOC are higher, indicating the onset of non-Newtonian flow at lower frequencies. Activation energies are also higher for the EOC-rich blends, because of the presence of long chain branching [2], with the exception of the 30/70 PP/EOC blend. At this composition, the zero shear viscosity showed significant positive deviation behaviour from the simple additivity rule, log $\eta_{0,b} = \sum_n^i w_i \log \eta_i$, where $\eta_{0,b}$ is the zero shear viscosity of the blend, η_i and w_i are the zero shear viscosities and weight fractions of blend component i, respectively, as demonstrated in Fig. 2. This blend is also significantly more elastic, as evidenced by comparing the relaxation times, shown in Table 2. These deviations may be due to differences in morphology compared to the rest of the blends. Specifically, the 30/70 PP/EOC composition displays different morphology than the respective PP/EBC blend, consisting of elongated filaments, as shown in Fig. 3.

It must be noted that even though the rest of the compositions follow the additivity rule quite closely, this should not necessarily be taken as evidence of miscibility [24].

Techniques used to provide evidence of phase separation in the melt involve the generation of Cole–Cole plots [25] and Han plots [26,27]. In this work, these techniques attested that all blends are immiscible. A representative example is shown in Fig. 4, which compares Han plots at three different temperatures for blends containing 30 wt% EOC. The substantial deviation from the terminal slope of 2

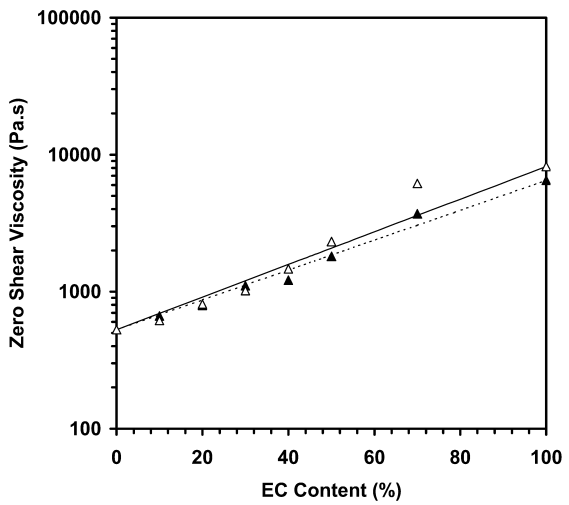

Fig. 2. Zero shear viscosities as a function of composition (210 °C); ▲ PP/EBC, △, PP/EOC, – – – –, rule of additivity for PP/EBC, —, rule of additivity for PP/EOC.

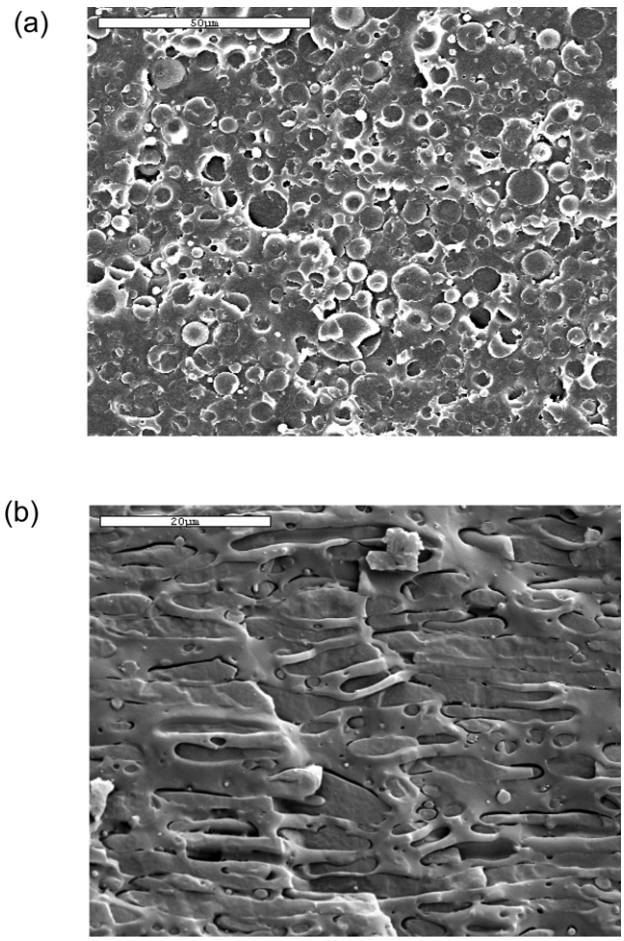

Fig. 3. Comparison of SEM images of batch-mixed blends (a) 30/70 PP/EBC, (b) 30/70 PP/EOC.

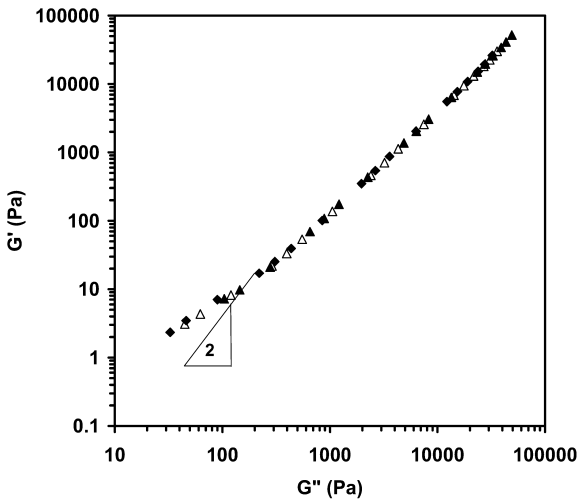

Fig. 4. Han plots of elastic modulus (G') versus loss modulus (G'') for PP/EOC 70/30 blend; ▲ 170 °C, △ 210 °C, ◆, 230 °C.

provides evidence of immiscibility in the temperature range studied.

3.2. Thermal properties

Fig. 5 shows typical DSC endotherms for the PP/EBC blends and Table 3 summarizes melting and crystallization temperatures for all blends. The inability to detect a peak for the EC phases at the 90/10 PP/EC compositions is probably due to inadequacy of the instrument to resolve the weak intensity of the peak. Even though the melting points of the PP phase remain relatively constant irrespective of composition, indicating the absence of any interactions such as co-crystallization within the PP phase, notable shifts in melting and crystallization temperatures are observed for the EC phase in the EBC blend.

To investigate the possibility of the shifts being due to partial miscibility between the two phases, the successive self-nucleation and annealing (SSA) technique [18], which is a thermal fractionation technique aiming at resolving molecular segregation in polymers exhibiting composition heterogeneity, was used. Fig. 6 compares DSC heating scans after SSA treatment for the 'unmixed' blends [18], which represent how the DSC melting scan would look if no interactions between components were present, to those of the melt mixed blends. The number of peaks in the two scans is virtually identical revealing molecular segregation of both components after SSA treatment, without miscibility.

Therefore, we propose that the observed shifts may be attributed to nucleation effects caused by the presence of PP crystals during the crystallization of the EC phase. Such nucleation effects have been reported previously in HDPE/ultra-low-density polyethylene blends [18]. Alternatively, the shifts may be due to broadening of the melting endotherms caused by the presence of different crystal sizes with various degrees of perfection [28].

Fig. 7(a) and (b) compares the crystallinities of the PP and EC components, respectively. For most compositions, the experimental data for PP displays a marked negative deviation from additivity, indicating that the PP phase is prevented from crystallizing in the blend in the presence of the ECs. It is worth noting that the EOC has higher crystallinity than the EBC, consistent with its higher density, even though it contains higher amounts of comonomer (see also Table 1).

Typical DMA traces of loss tangent, tan δ, as a function of temperature for the PP/EBC system are shown in Fig. 8 and glass transition temperatures, determined from the maxima of these traces, are summarized in Table 3. The maximum of the EC glass transition shifts toward lower temperatures as EC content decreases (Table 3), in agreement with previous observations [14]. These shifts may be due to limited partial miscibility of the components in their amorphous state.

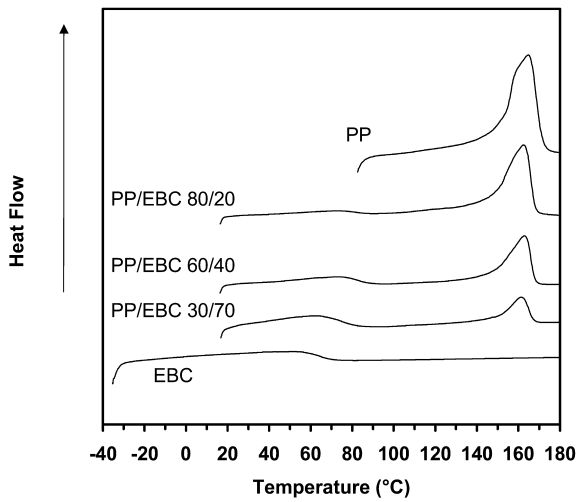

Fig. 5. DSC endotherms for PP/EBC system.

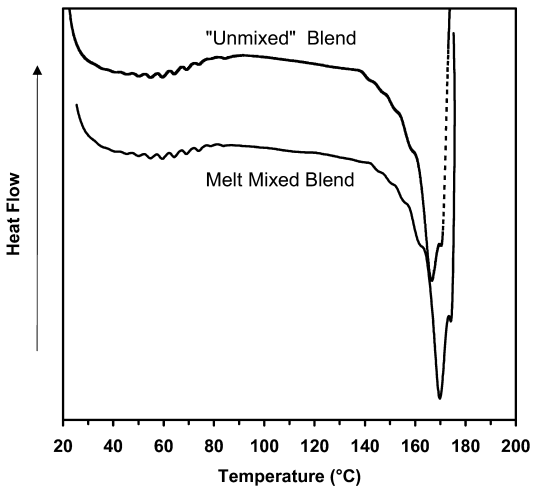

Fig. 6. DSC heating traces after SSA fractionation for 'unmixed' and melt mixed PP/EBC blends.

Table 3
Thermal properties

Blend PP/EC	EBC						EOC					
	T_m (°C)		T_c (°C)		T_g (°C)		T_m (°C)		T_c (°C)		T_g (°C)	
	EBC	PP	EBC	PP	EBC	PP	EOC	PP	EOC	PP	EOC	PP
100/0		164.7		109.8		3		164.7		109.8		3
90/10		163.1		110.3		3		163.7		109.0		3
80/20	71.1	162.6	59.9	113.2	−63	3	73.2	164.1	59.2	112.4	−68	4
70/30	71.8	163.5	59.1	110.1	−57	6	72.8	163.2	59.0	112.8	−69	−5
60/40	72.1	163.0	59.9	111.8	−58	6	72.3	163.2	59.5	111.6	−69	1
50/50	62.9	163.8	49.1	110.0	−59	6	72.4	163.7	58.5	108.0	−69	−15
30/70	61.0	161.2	49.8	102.0	−46	6	72.8	161.7	60.7	97.2	−60	3
0/100	50.9		38.5		−45		72.1		56.4		−50	

3.3. Morphology and mechanical properties

SEM images of PP/EBC blends, produced using the twin-screw extruder, reveal droplet-matrix morphologies, as shown in Fig. 9. In spite of the high viscosity ratio characterizing these systems (9.2 for PP/EBC and 5.6 for PP/EOC calculated at a nominal shear rate of 100 s^{-1}), no evidence of coalescence appeared as EC content increased. Relatively uniform particle size distributions were obtained with average particle sizes ranging from 1.3 to 2 μm and polydispersities not exceeding 1.3. The number and volume average diameters, D_n and D_v, respectively, for the PP/EC 70/30 compositions of both systems, are summarized in Table 4. The particles are generally larger than reported previously for systems with lower viscosity ratios [10,14] and the average diameter of the PP/EOC system is slightly higher. Phase inversion occurs when EBC content is above 50% and EBC becomes the matrix phase at PP/EBC 30/70 composition.

Increasing EBC content affects mechanical properties of these blends decisively. This is evident in Table 5, which

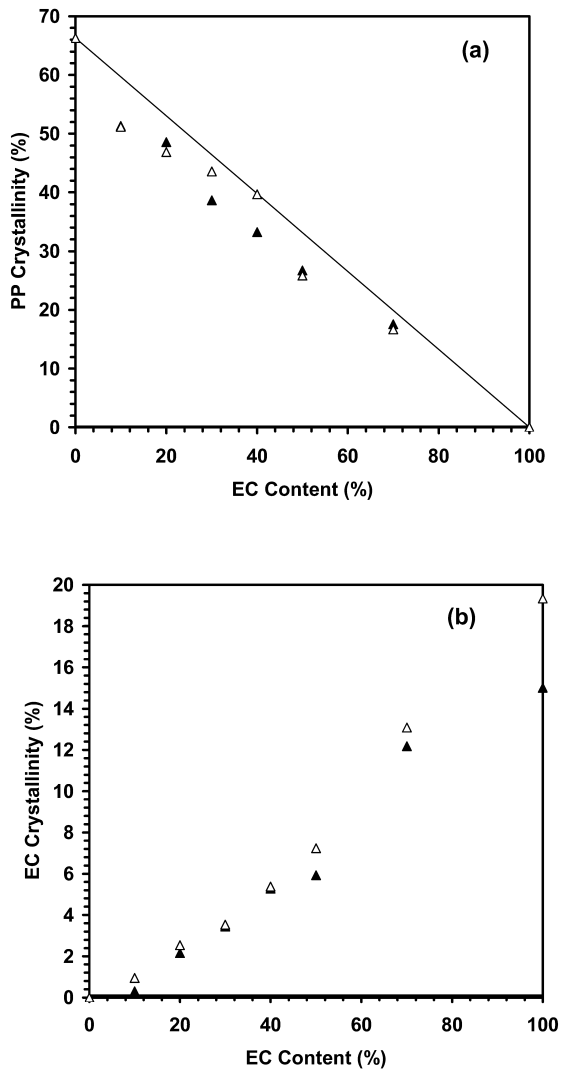

Fig. 7. (a) PP crystallinity as a function of blend composition; ▲ PP/EBC, △ PP/EOC, — rule of additivity. (b) EC crystallinity as a function of blend composition; ▲ PP/EBC, △ PP/EOC.

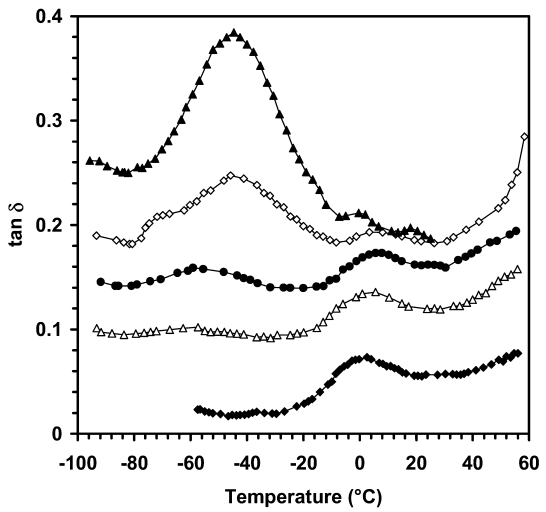

Fig. 8. DMA traces of loss tangent, tan δ, as a function of temperature for the PP/EBC system; ◆ PP, △ PP/EBC 70/30, ● PP/EBC 50/50, ◇ PP/EBC 30/70, ▲ EBC.

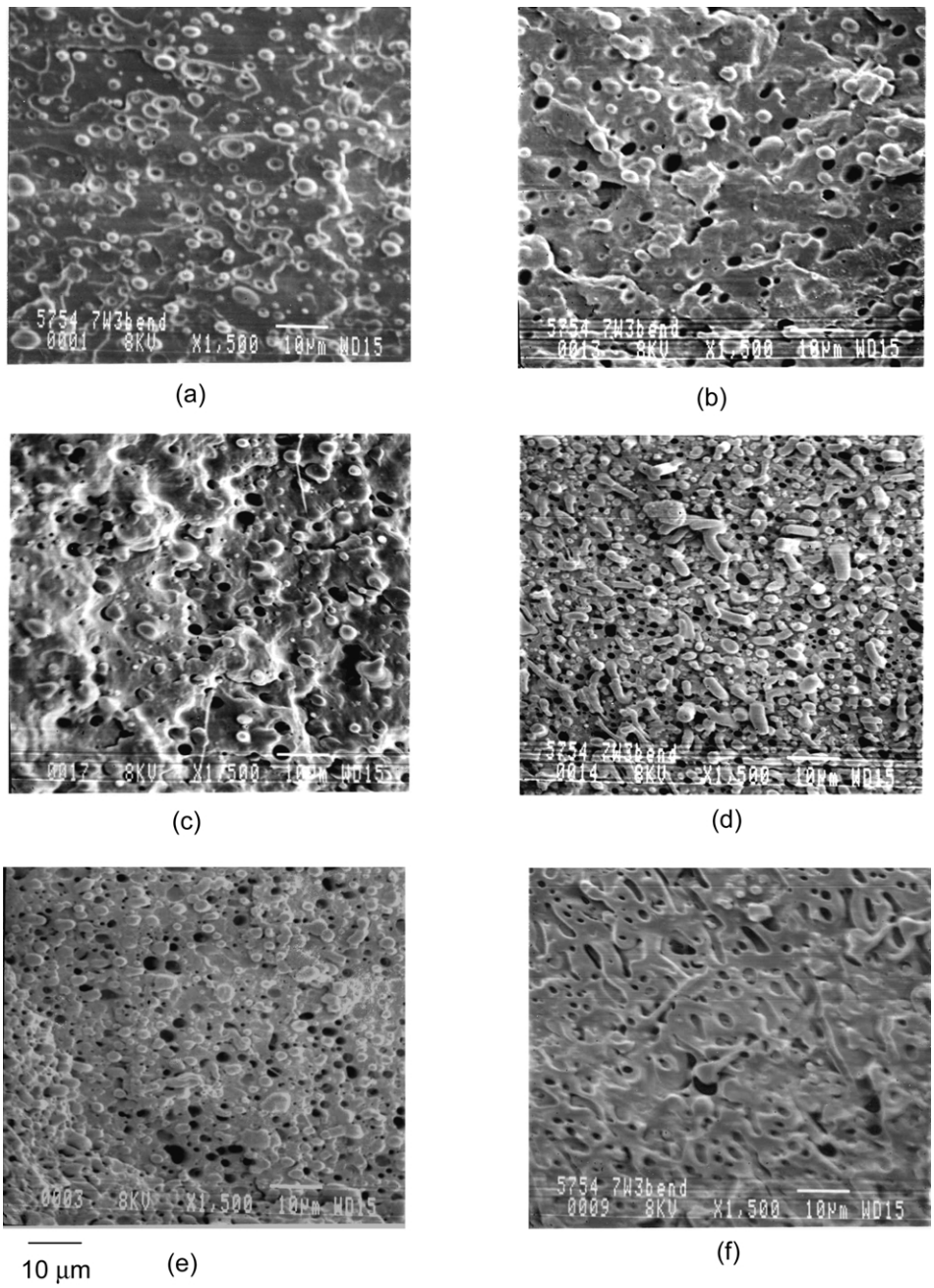

Fig. 9. SEM images of PP/EBC blends prepared by twin-screw extrusion; (a) PP/EBC 90/10, (b) PP/EBC 80/20, (c) PP/EBC 70/30, (d) PP/EBC 60/40, (e) PP/EBC 50/50, (f) PP/EBC 30/70.

Table 4
Average particle sizes, Palierne and Wu model predictions (70/30 composition, 210 °C)

	PP/EBC	PP/EOC
D_n (μm)	1.57	2.05
D_v (μm)	2.01	2.41
σ (N/m)	0.00064	0.0006
Viscosity ratio at 100 s^{-1}	9.15	5.6
D_n predicted by Eq. (4)	0.77	0.5

depicts the variation of impact and tensile properties for the same blend compositions, as the ones shown in the SEM images of Fig. 9. A substantial increase in elongation at break and impact energy is seen at 50/50 composition, whereas no failures were observed above this composition. This transition from plastic to elastomeric properties is clearly associated to the higher EBC content and the ensuing phase inversion, which results in EBC being the matrix component.

Although similar results in tensile properties were obtained for the PP/EOC blends, it must be noted that the butene-based EBC proved to be more effective in improving

Table 5
Mechanical properties of PP/EBC blends

Blend PP/EBC	Stress at yield (MPa)	Elongation at break (%)	Impact energy (kJ/m^2)
100/0	39.2 ± 1.2	36.1 ± 6	1.8 ± 0.58
90/10	19.2 ± 1.1	102 ± 7	1.1 ± 0.46
80/20	14.3 ± 1	138 ± 5	2.4 ± 0.74
70/30	15.9 ± 0.3	128 ± 19	2.9 ± 0.27
60/40	13.2 ± 8.4	123 ± 13	5.2 ± 1.24
50/50	11.8 ± 0.2	131 ± 9	17.6 ± 4.10
30/70	No yield	No break	No break
0/100	No yield	No break	No break

the impact properties of PP than the octene-based EOC. For example, at 30% POP content, the impact energy of PP/EOC was 34% lower than that of PP/EBC. Since the morphologies of these blends are very similar, the lower impact energy in the PP/EOC blends may be due to their higher crystallinity (see Fig. 7).

3.4. Interfacial tension

The Palierne emulsion model [22,29,30] was used to fit the viscoelastic curves of the blends. A representative fit is shown in Fig. 10 for the 70/30 PP/EBC blend. The resulting values of interfacial tension, σ, for 70/30 PP/EC compositions at 210 °C, summarized in Table 4, are virtually identical and in good agreement with those reported previously for similar systems [12,31]. According to the Helfand and Tagami theory for immiscible polymers [32,33], knowledge of the interfacial tension, σ, can provide an estimate of the Flory–Huggins interaction parameter, χ:

$$\sigma = (\chi/6)^{1/2} b \rho_0 kT \tag{2}$$

where b is the effective length per monomer unit, ρ_0 is the density of the pure polymer; K is the Boltzmann constant; and T is the temperature. In addition, the equilibrium interfacial thickness, b, between two immiscible polymers can be expressed as:

$$\beta = \frac{kT}{3b\sigma} \tag{3}$$

Based on the above, it can be deduced that the Flory–Huggins interaction parameters and interfacial thicknesses for the two systems should be similar.

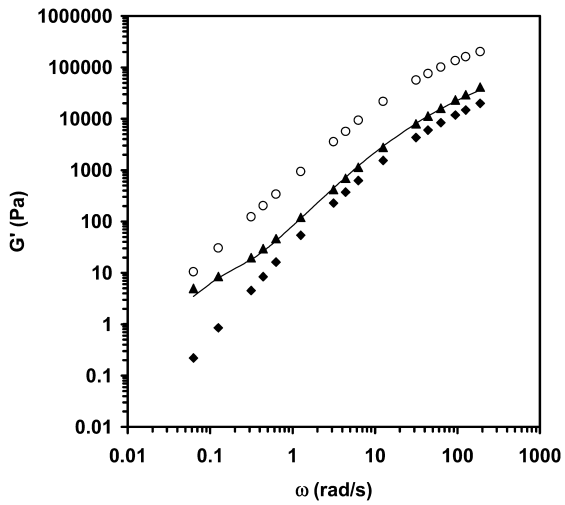

Fig. 10. Palierne model fits for PP/EBC 70/30 blend at 210 °C; ◆ G' of matrix PP, ○ G' of droplet EBC, ▲ G' of PP/EBC 70/30 blend; — Palierne model fit.

3.5. Morphology evolution during shearing

The well known empirical model proposed by Wu [34] is frequently used to determine the size of the dispersed phase obtained by extrusion:

$$\frac{\dot{\gamma}\eta_m D_n}{\sigma} = 4\left(\frac{\eta_d}{\eta_m}\right)^{\pm 0.84} \tag{4}$$

where $\dot{\gamma}$ is the shear rate, σ the interfacial tension, D_n the number average diameter of droplets, η_d and η_m is the viscosity of droplet and matrix, respectively; the plus sign in the exponent applies for $\eta_d/\eta_m > 1$ and the minus sign applies for $\eta_d/\eta_m < 1$.

Predictions obtained by applying the Wu model are stated in Table 4. The discrepancy between model predictions and experimental results is possibly due to coalescence effects that are not taken into account by the model.

Since these blends are almost always subjected to some form of post-processing operation involving further shearing, the effect of shearing on the morphology of the extruded samples was studied under simple shear flow using the parallel plate rheometer. Even at stress levels as low as 25 Pa, shearing resulted in significant deformation of the dispersed phase, leading to fibril formation and subsequently to breakup and appearance of some sub-micron particles, as shown in Fig. 11. Fibrillar morphology, without breakup, was observed for the PP/EBC 70/30 composition. Number average sizes of these particles as a function of strain at two levels of stress are summarized in Fig. 12. According to Grace [35] no particle breakup can occur at viscosity ratios above 3.5 under simple shear flow. Excellent adhesion between the two phases may be responsible for generating shear forces capable of deforming the dispersed droplets in the systems under consideration, therefore enabling the generation of fine morphologies even at high viscosity ratios.

4. Conclusions

Blends of PP with ethylene-α-butene and ethylene-α-octene copolymers are immiscible over the whole range of compositions in the melt and solid state. Low interfacial tension between the phases suggests excellent mechanical compatibility, which is also manifested by significant

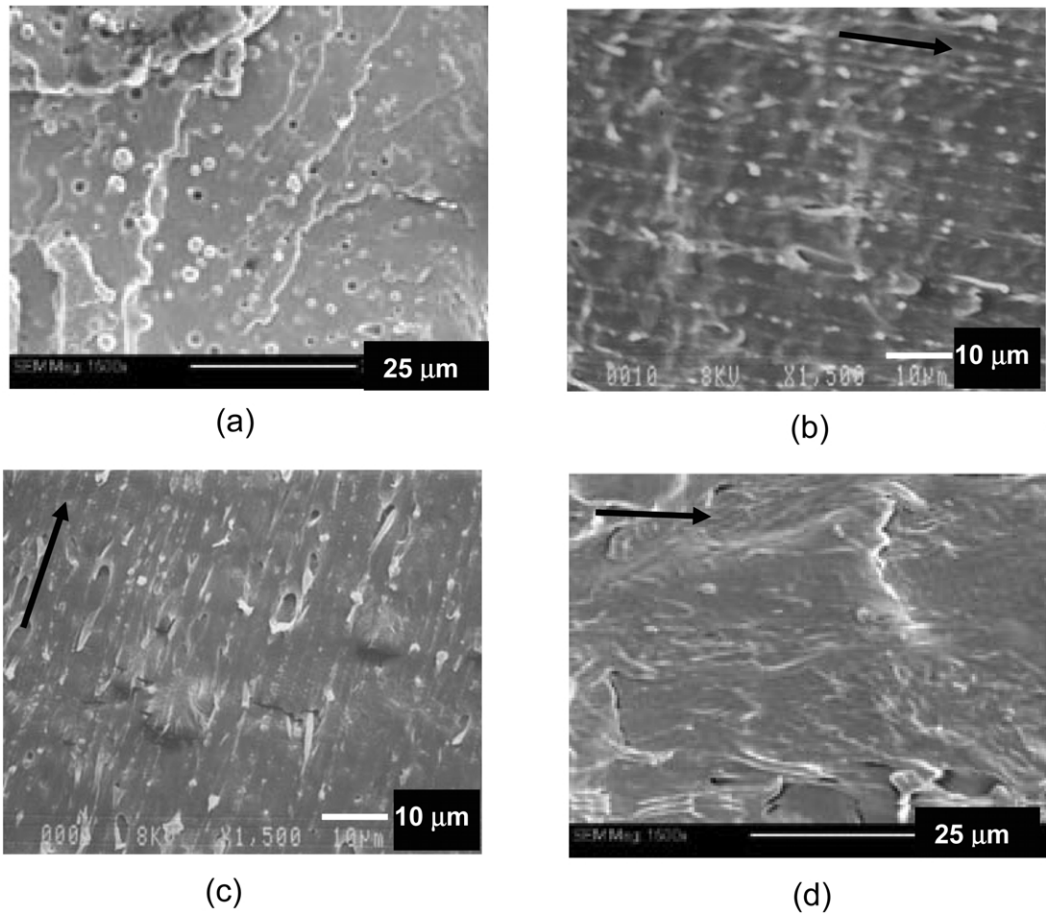

Fig. 11. SEM images of PP/EBC blends after simple shearing: (a) 90/10 PP/EBC before shearing; (b) 90/10 PP/EBC, shear stress 25 Pa, strain 100; (c) 90/10 PP/POP, shear stress 100 Pa, strain 100; (d) 70/30 PP/POP, shear stress 25 Pa, strain 400. Arrows indicate direction of shear.

improvements in ductility upon addition of ECs into the PP matrix. There are no substantial differences in interfacial tension, therefore compatibility and phase adhesion, between the butene and octene-based systems.

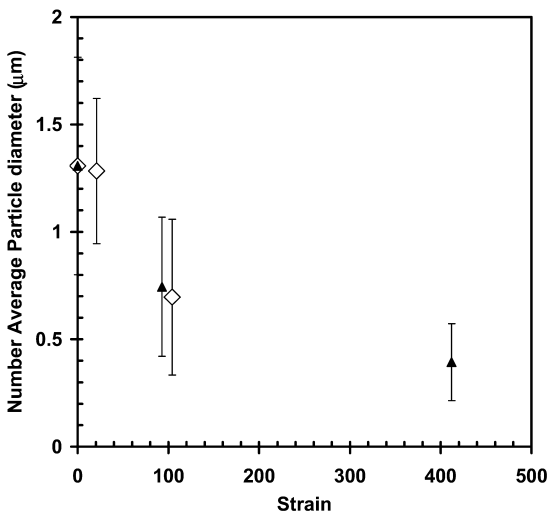

Fig. 12. Number average diameter of dispersed droplets for PP/EBC blends after shearing experiments as a function of total strain at different stress levels; ◇ 25 Pa, ▲ 100 Pa.

Morphology has a significant effect on mechanical properties; transition from plastic to elastomeric properties is observed above 50% composition, which coincides with phase inversion. Post-extrusion shearing, even at very low levels of stress, alters dramatically the morphology, resulting in the formation of elongated fibrils and sub-micron particles.

Acknowledgements

The authors would like to acknowledge Imperial Oil Ltd, ExxonMobil Chemical, The Centre for Automotive Materials and Manufacturing, The Canada Foundation for Innovation (CFI) and The Ontario Innovation Trust (OIT) for supporting this work. The contributions of Dr T.C. Yu of ExxonMobil Chemical are gratefully acknowledged.

References

[1] Kim YS, Chung CI, Lai SY, Hyun KS. J Appl Polym Sci 1996;59: 125–37.
[2] Starck P, Malmberg A, Löfgren B. J Appl Polym Sci 2002;83: 1140–56.

[3] Wood Adams PM, Dealy JM, deGroot AW, Redwine OD. Macromolecules 2000;33:7489–99.
[4] Chen F, Shanks R, Amarasinghe G. J Appl Polym Sci 2001;81: 2227–36.
[5] Kwag H, Rana D, Cho K, Rhee J, Woo T, Lee B, Choe S. Polym Engng Sci 2000;40(7):1672–81.
[6] Liu C, Wang J, He J. Polymer 2002;43:3811–8.
[7] Lee H, Cho K, Ahn T-K, Choe S, Kim I-J, Park I, Lee BH. J Polym Sci Part B: Polym Phys 1997;35(10):1633–42.
[8] Da Silva ALN, Tavares MIB, Politano DP, Coutinho FMB, Rocha MCG. J Appl Polym Sci 1997;66:2005–14.
[9] Da Silva ALN, Rocha MCG, Coutinho FMB, Bretas R, Scuracchio C. J Appl Polym Sci 2000;75:692–704.
[10] Kukaleva N, Jollands M, Cser F, Kosior E. J Appl Polym Sci 2000;76: 1011–8.
[11] Kukaleva N, Cser F, Jollands M, Kosior E. J Appl Polym Sci 2000;77: 1591–9.
[12] Dharmarajan NR, Yu TC. Plast Engng 1996;52(8):33–5.
[13] Yu TC. Polym Engng Sci 2001;41:656–71.
[14] McNally T, McShane P, Nally GM, Murphy WR, Cook M, Miller A. Polymer 2002;43:3785–93.
[15] Yamaguchi M, Miyata H, Nitta KH. J Appl Polym Sci 1996;62: 87–97.
[16] Yamaguchi M, Miyata H, Nitta KH. J Polym Sci Part B: Polym Phys 1997;35:953–61.
[17] Yamaguchi M, Miyata H. Macromolecules 1999;32:5911–6.
[18] Arnal ML, Sánchez AJ, Müller AJ. Polymer 2001;42:6877–90.
[19] Fillon B, Wittmann JC, Lotz B, Thierry A. J Polym Sci Part B: Polym Phys 1993;31:1383–939.
[20] Martin P, Carreau PJ, Favis BD, Jérôme R. J Rheol 2000;44(3): 569–83.
[21] Brown GM, Butler JH. Polymer 1997;38:3937–45.
[22] Carreau PJ, De Kee DCR, Chhabra RP. Rheology of polymeric systems. Munich: Hanser; 1997.
[23] Macosko CW. Rheology: principles, measurements, and applications. New York: Wiley; 1994.
[24] Utracki LA, Schlund B. Polym Engng Sci 1987;27:1512–22.
[25] Dumoulin MM, Utracki LA, Carreau PJ. Melt rheology and morphology of linear low density polyethylene/polypropylene blends. In: Utracki LA, editor. Two-phase polymer systems. Munich: Hanser; 1991. p. 185–212.
[26] Han CD, Kim YJ, Chuang HK. J Appl Polym Sci 1983;28:3435–51.
[27] Kim JK, Lee HH, Son HW, Han CD. Macromolecules 1998;31: 8566–78.
[28] Simanke AG, Galland GB, Freitas L, da Jornada JAH, Quijada R, Mauler RS. Polymer 1999;40:5489–95.
[29] Palierne JF. Rheol Acta 1990;29:204–14.
[30] Graebling D, Muller R, Palierne JF. Macromolecules 1993;26:320–9.
[31] Carriere CJ, Silvis HC. J Appl Polym Sci 1997;66:1175–81.
[32] Helfand E, Tagami Y. J Polym Sci B: Polym Lett 1971;9:741–6.
[33] Yamaguchi M. J Appl Polym Sci 1998;70:457–63.
[34] Wu S. Polym Engng Sci 1987;27:335–43.
[35] Grace HP. Chem Engng Commun 1982;14:225–77.